

Computational performance of a-100 kW low pressure turbine to recover gas turbine exhaust energy

A A Ahmad Zahidin¹, A M I Mamat^{1*}, A Romagnoli²

¹Faculty of Mechanical Engineering, Universiti Teknologi MARA,
40450, Shah Alam, Selangor, Malaysia

*Email: amanihsan@salam.uitm.edu.my

²Nanyang Technological University, 50, Nanyang Ave,
Singapore 639798, Singapore

ABSTRACT

A low pressure turbine was designed to recover exhaust energy from internal combustion engine. The turbine is located downstream retrieved exhaust heat energy from combustion after flowing through the high-pressure turbine in the turbocharging system. The work output obtained from the exhaust energy is used to drive an electric generator with power output of 1.0kW. These was not done by commercial turbine as the low efficiency resulted when operated. The main purpose of this project is to develop a scaling model for low pressure turbine with power output up to 100kW. An existing low pressure turbine was used as a guideline to upscale the turbine. The scaling factor was obtained by comparing the baseline with the required power output. The turbine performance was analysed by using a commercial computational fluid dynamic software namely, ANSYS® CFX Version 17.0. The study found that the scaling factor, f of 10 can be used to produce a 100kW at passage. Thus, the geometrical parameter will be scaled accordingly. The rotational speed was reduced from 50,000 rpm to 5,000 rpm. The CFD analysis found the peak total-static efficiency (η_{t-s}) is 81% at the pressure ratio (PR) of 1.12 which has produced the turbine power of 119.88 kW. Despite the LPT swallowing capacity is increased from 0.05 kg/s to 5.0 kg/s, the LPT is limited by the operational choking PR which is 1.4. In conclusion, the computational analysis has shown that the scaling process is capable to produce a similar turbine characteristics between the baseline turbine and the upscale turbine.

Keywords: Energy recovery; turbomachinery; turbocompounding

INTRODUCTION

Transportation sector uses more than 50% of the world's fossil fuel and The Energy Institute expects the growth to continue until 2040 [1]. The fossil fuel is refined from the petroleum crude oil that is depleted with continuous usage [2]. Alternative renewable liquid fuels such as biofuels are proposed by many researchers to replace the fossil fuels [3]. Despite the high demand for fuels in the transportation, well-to-wheel energy efficiency is approximately 14% only [4]. The energy in the fuel is wasted by many various losses and more than 33% of the fuel energy is released in the form of exhaust gas [5]. Many engine technologies are

developed to improve the engine efficiency and minimise the carbon emission due to stringent governmental policies [6-9]. Thus, recovering energy losses will exploit the fuel energy on a vehicle at its optimum potential and increase the combustion efficiency [10].

One of the realistic idea is to optimize the fuel energy from the combustion process is by recovering the exhaust energy [11]. The exhaust energy can be recovered by using three technologies; (1) organic Rankine cycle (ORC)[12], (2) thermoelectric generator (TEG) [13] and (3) turbocompounding [13-15]. The ORC system requires a large space on the engine bay and the TEG materials are expensive [16]. A comparative study between ORC and turbocompounding on a diesel engine by Adwari et al. [17] has shown that the energy recovery system has reduced the fuel usage as much as 5% and 8%, respectively. The turbocompounding is operated by mounting additional turbine downstream of the turbocharging system [18]. This downstream turbine is known as low pressure turbine (LPT) that retrieves waste heat from upstream turbine (high pressure turbine) [10, 19].The turbocompounding is by far the best choice compare to ORC and TEG due the bolt-on concept to simplify the assembly process and the manufacturing cost is cheaper than the other two concepts [10, 20-24].

The turbocompounding system can be divided into two main categories: mechanical and electrical turbocompounding. The former feeds back the excess energy recovered from the exhaust gases directly into the engine crankshaft whereas the latter uses the recovered energy in order generate electricity which can be used to power electric auxiliaries present in a vehicle or recharge battery packs [17, 25]. The mechanical turbo-compound system that was done by Voith on segment of heavy-duty for commercial vehicles has resulted in savings of fuel approximately 8% to 9% depending on different operating profile [20]. Rather than using mechanical linkage and power transmission in mechanical turbocompounding, the system for electric turbocompounding uses an electric generator run by low pressure turbine (LPT) [26]. This system reduces the losses created by the mechanical linkages coupler for mechanical parts. However, a slight increment of back pressure is observed in the exhaust tail [27].

Another variation of electric turbo-compound is the so called electric assisted turbocharger (ETA) [28]. This consists of an electric machine directly coupled to the shaft of the main turbocharger which can be used either as an electric generator (=recovering energy from the exhausts) or an electric motor (=adding energy to the turbocharger shaft during transient operation) [28]. However, a higher exhaust temperature can be dissipated from the turbine and restrict the power electronic operations which must be lower than 200°C. Therefore, the ETA is not suitable for a small petrol engine due for that reason [29]. The recovered energy can power up batteries, electrical unit and other auxiliary unit[30]. The power conversion by turbo-compound is directed back to power the engine and the extra power are redirected to auxiliaries of the vehicle [31]. But, constraints exist for electric turbocompounding systems are due to the electric machine that needs to run at a higher speed over the entire engine driving cycle in order to work efficiently [32].

The electric turbocompounding can be used to recover the exhaust gas from gas turbine which is used to drive electric generator in power-plant station [33]. Some power-plants are designed with a combined cycle where a Rankine cycle is used to recover heat energy from the gas turbine [34]. Thus, the cycle efficiency is better. However, there are some energy are wasted as low-grade energy in the exhaust gas. The low-grade energy is contained of hot gas with low pressure condition. Low pressure turbine can be used to recover

the low grade energy in the exhaust gas. However, the current design for the low pressure turbine was designed to produce mechanical work at 1.0 kW and operates at 50,000 rpm. A turbine scaling method which was developed by Kant et al. [31] can be used to upscale the power output of the baseline turbine from 1.0kW to 100kW. Despite increasing the power output and physical dimensions, the proposed scaling method must maintain the characteristics of the baseline turbine.

Main of objective of this paper is to evaluate the performance of the upscale 100kW turbine. In the first methodology of the research work, a numerical scaling method was used to get the suitable scaling factor, f . Then, the physical geometry of the upscale turbine was generated in 3 dimensional computer aided design modelling to produce a single-passage turbine meshing. The meshing independence study was done to identify the suitable meshing quantity for the computational analysis. A commercial computational fluid dynamics (CFD) namely Ansys® CFX version 17.0 was used to generate the turbomachinery computational data. Finally, the computational turbine performances such as pressure ratio (PR), mass flow parameter (MFP), velocity ratio (VR) and total-to-static efficiency (η_{t-s}) was generated for three turbine speeds; 4000 rpm, 5000 rpm and 6000 rpm.

METHODOLOGY

Scaling turbine performance and geometry

Turbine performance maps are portrayed by a numerous number of working operating point. Each operating point is characterized by a particular arrangement of information comprising of a mass flow, rotational speed and efficiency. Kant et al. developed the characteristic of LPT performance map scale with a greater mass flow capacity [31]. As the specific turbine geometry is kept unchanged, the turbine size also has to increase. Thus, each operating point need to be increased by mass flow scaling factor x . Geometric parameter of LPT also sequentially scaled by scaling factor f . Turbine performance maps are scaled without changing the inlet conditions. In order to simplify the scaling method and process, gas properties (pressure, temperature, velocity and gas composition) at inlet were maintained. The efficiency and stresses of blade speed were not effected in the first-order accuracy. It is essential to scale the turbine with the increasing of mass flow capacity. Equation (1) shows the mass flow at rotor inlet;

$$\dot{m} = \rho C_2 A_2 \quad (1)$$

Due to constant exhaust gas properties, flow path area A_2 has to increase as the mass flow capacities are increased by x times. Equation (2) shows that A_2 is the area inlet of rotor, D_2 as diameter of rotor inlet and Z_2 as rotor inlet blade height.

$$A_2 = 2\pi \frac{D_2}{2} Z_2 \quad (2)$$

Thus, every geometric parameter needs to be scaled by factor f ,

$$\dot{m}_{base} x = \rho C_2 2\pi \frac{f D_{2,base}}{2} f Z_{2,base} \quad (3)$$

$$x = f^2 \quad (4)$$

From equation (4), it leads to

$$\dot{m}_{scaled} = f^2 \dot{m}_{base} \tag{5}$$

Equation (5) shows that the scaled mass flow rate is by the factor of square from the baseline turbine. Also, the scaling of the mass flow rate is highly sensitive to the turbine power output. Figure 1 shows the sensitivity of the mass flow rate to the turbine power. By using the polytropic equation, the Pressure Ratio, PR was assumed at 1.1 and the inlet temperature was 1100 K, the turbine power was calculated and the result is shown in the Figure 1. The turbine power is linearly increased as the mass flow rate is increased. From the Figure 1, the 100 kW turbine power output can be achieved if the mass flow rate is scaled up from 0.05 kg/s to 5.0 kg/s.

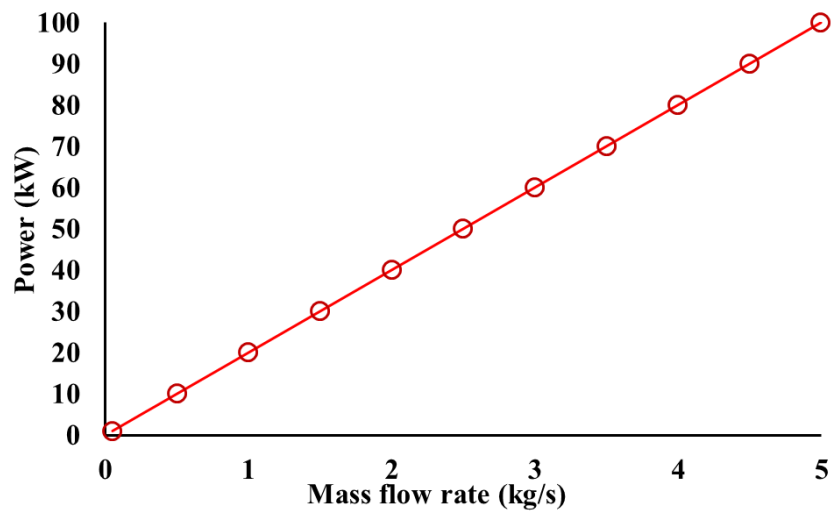


Figure 1. Turbine power output against the mass flow rate, \dot{m} .

Walsh previous published work assumed an existing turbine could be scaled by set of scaling group [19]. Equation (6) seems to be reliable with the previous work published by [19].

$$D_{scaled} = f D_{base} \tag{6}$$

Exhaust gas properties are constant as stated before, rotational speed N can be obtained with function of diameter in Equation (7)

$$\frac{D_{2,scaled}}{N_{scaled}} = \frac{D_{2,base}}{N_{base}} \tag{7}$$

Relate equation (7) with scale factor f ,

$$N_{scaled} = \frac{N_{base}}{\sqrt{x}} = \frac{N_{base}}{f} \tag{8}$$

Equation (8) shows that the turbine rotation is inversely proportional to the scale factor. As the scaling mass flow rate is increased by the factor of square, the rotation will be reduced as the mass flow is increased. The Figure 2 shows the turbine rotational speed, N vs the mass flow rate, \dot{m} .

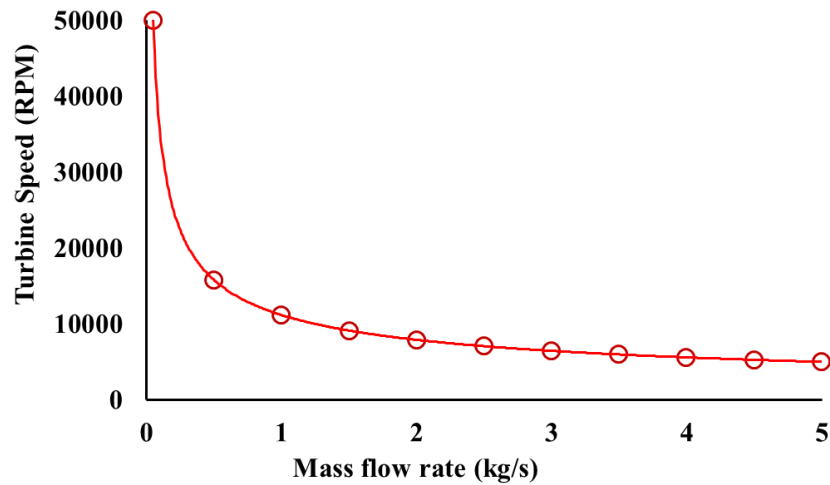


Figure 2. Turbine rotation speed, N against mass flow rate, \dot{m} .

The physical parameter of the turbine and the design point were obtained from the given equations. The turbine power output is scaled from 1 kW to 100 kW with the scaling factor of 10. Thus, the mass flow rate is increased to 5.0 kg/s and the rotational speed is reduced to 5,000 rpm. The turbine radius at root mean square, r_{rms} is increased from 30.1 mm to 301 mm. The Pressure Ratio, PR, Total Inlet Temperature, T_{01} and the Specific Power Coefficient, S_w are maintained at the design point.

Table 1. Base and scale unit parameter.

Variable/ Parameter	Base	Scaled
Power output (kW)	1	100
Area (mm ²)	0.0034	0.344
Mass flow rate (kg/s)	0.05	5.00
Radius root mean square at inlet, $r_{rms,2}$ (mm)	30.1	301.0
Radius root mean square at outlet, $r_{rms,3}$ (mm)	12.3	123.0
Number of blades	9	9
Speed (rpm)	50,000	5,000
Pressure ratio, PR	1.1	1.1
Total inlet temperature at, T_{01} (K)	1100	1100
Specific power coefficient, S_w	0.013	0.013

The velocity triangle at the inlet and outlet of the turbine are maintained. The turbine layout and the velocity triangle at the inlet and outlet of the turbine are shown in Figure 3(a) and Figure 3(b). Subscript 1 and 3 is referred to volute inlet and rotor outlet; respectively. Subscript 2 is referred to rotor inlet as shown in the Figure 3(a). Based on the Figure 3(b), variable C presents absolute velocity of the blade, W presents relative velocity whereas U represents the blade speed. The symbol α is symbolised absolute angle to present reference angle on LPT meanwhile β presents velocity for relative velocity. i is incidence angle between the relative angle, β_2 and the blade angle, β_b at the leading edge. All of the velocity components are kept similar using the scaling factor method.

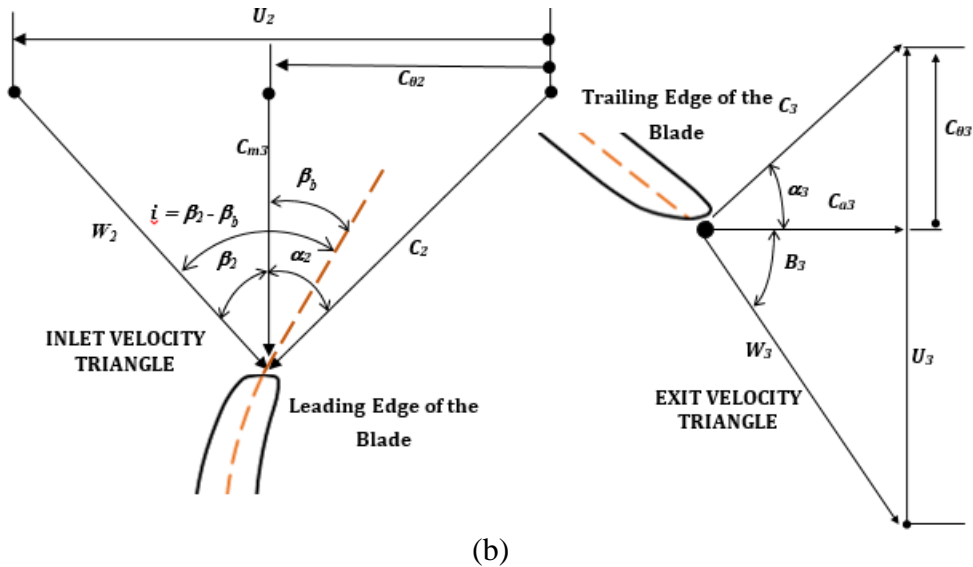
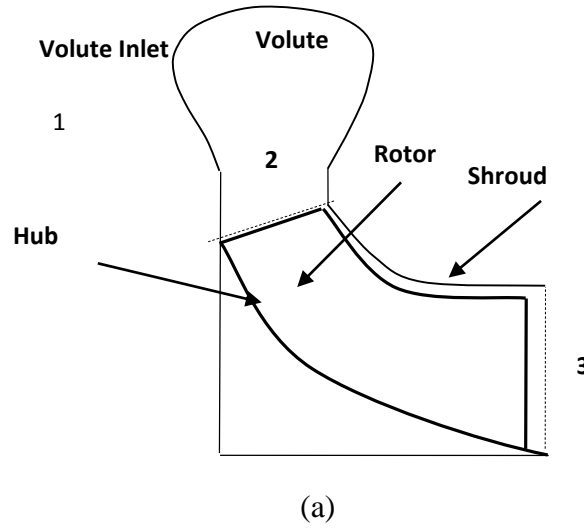


Figure 3. Turbine geometry (a) turbine layout (b) velocity triangle for inlet and outlet of radial turbine.

3D turbine blade configurations

A method for configuring blade profile is defined by using 4th degree Bezier polynomial curve that consists of seven profile which are hub, shroud, mean, low mean, upper mean, upper base and low base. Figure 4 (a) shows the blade profiling. The projection of the camberline curvatures was done by using the Bezier Polynomial with reference of cylindrical radius on blade profile define the radial fibre element in the mixed-flow turbine. By fixing the camberline angle which is -45° between the hubs to shroud, the lean angle of the turbine blade was obtained. Leading edge is maintained at constant fixed angle and the trailing edge of the blade is varied. Figure 4 (b) shows the camberline profile. The 3D points for the turbine were generated for the suction surface and the pressure surface after setting the turbine thickness.

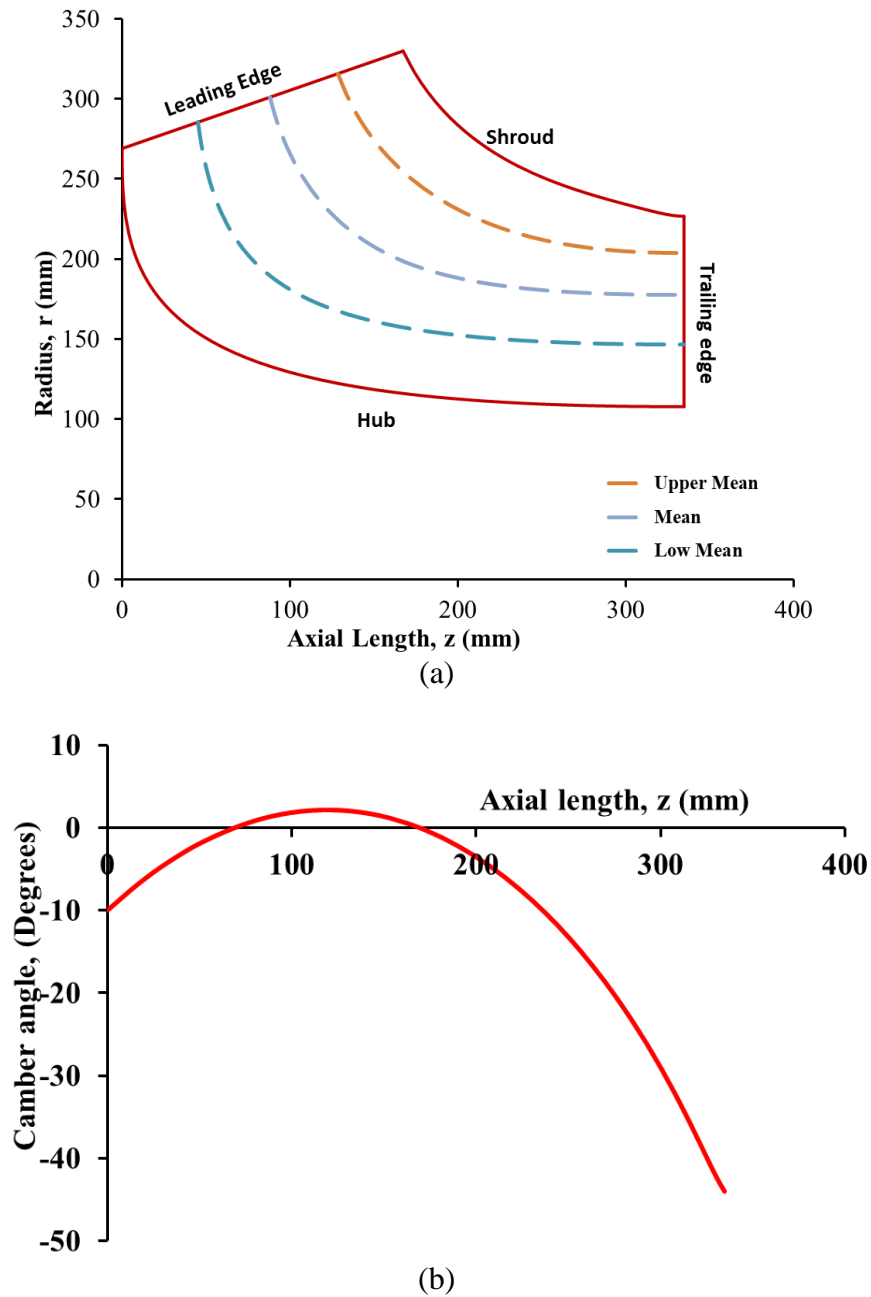


Figure 4. Blade and camberline profiling (a) blade profile (b) camber angle for the blade profile.

Computational fluids dynamics (CFD) setup

The CFD analysis was done by using a single passage condition. There are three processes were done for the CFD analysis which are; (1) generate turbine meshing, (2) Pre-processing and (3) CFD post processing. The modified turbine will generate mesh then export to CFX-Pre for several boundaries input. Finally, the simulation result is analysed in the CFD-Post.

The meshing process of the turbine element was done by using Turbogrid. Prior to the off-design turbine performance, mesh independent study was conducted to analyse the

meshing sensitivity. The CFD analysis for meshing nodes from 100,000 to 1,000,000 was conducted and the turbine total-to-static efficiency was analysed. Figure 5 shows the results of the Total-to-static efficiency against the total meshing nodes. It can be seen in the Figure 5 that the turbine efficiency is constant when the total number of meshing nodes is higher than 200,000. As a result, the total number for the meshing nodes was set at 200,000 because the turbine efficiency result is sufficient and the duration to run the simulation is at minimum.

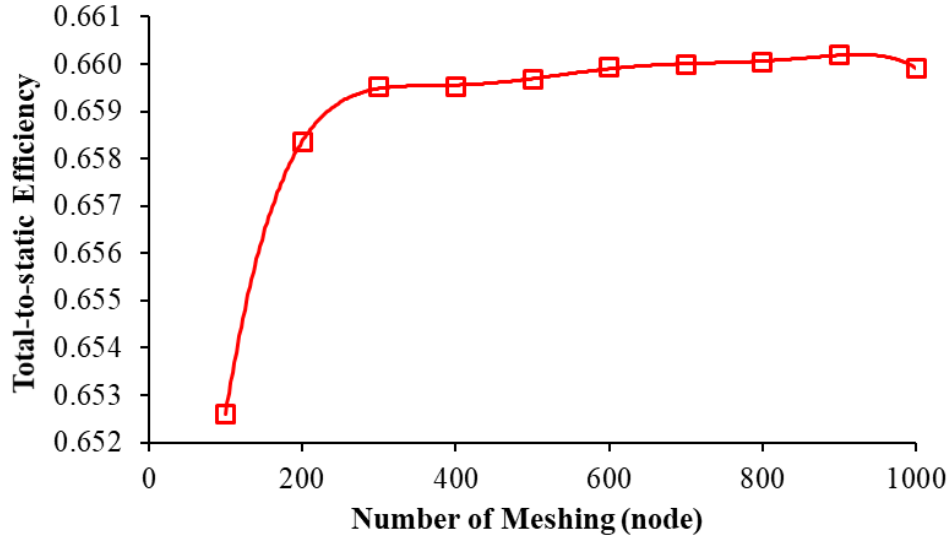
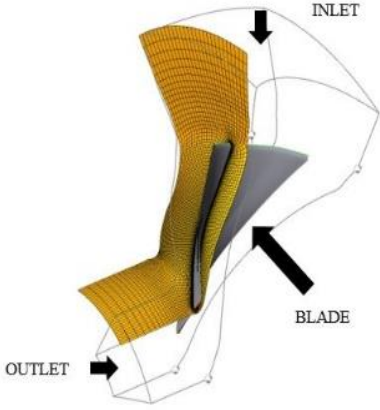


Figure 5. Total-to-static efficiency vs total meshing nodes.

Table 2. Single passage mesh statistics.

Domain	Nodes	elements
Passage	237 202	225 333
Inlet	9918	8288
Outlet	17 556	15 392
Total	264 676	245 013



Meshing Elements

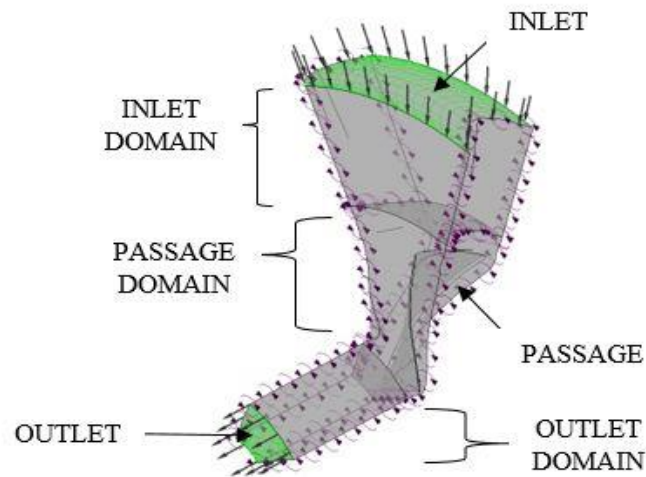


Figure 6. Boundary interface of turbine.

The meshing method was done by using Target Passage Mesh Size with nodes and elements used in each component in the analysis are shown in Table 2. Meshing method was optimized at wall using absolute method. The set up for the pre-processing was done in the CFX-pre where the input for boundary conditions were given. Figure 6 shows the boundary interface for the turbine meshing. For the inlet boundary condition, the swirling angle was fixed into 77° . The input for inlet was set as mass flow rate which is 5 kg/s divided by the number of blade existed with flow direction of cylindrical component which consist of three components, radial tangent and axial. However, it was assumed that only radial and tangential component were existed while the flow axial component was presumed to be 0. The material was set to be an ideal gas with value of specific heat $C_p = 1559.9 \text{ J/kg/K}$ at constant pressure and the static temperature is set at 1100 K. For outlet section, the opening static pressure and ambient temperature were set to $P = 100 \text{ kPa}$ and $T = 298 \text{ K}$ and the flow was assumed to be normal to the exit area. The analysis was done at 3 different operating speeds; 4000 rpm, 5000 rpm and 6000 rpm with medium turbulence (5%). Once all the inlet and outlet boundary conditions were set, the simulation process of the solver need to be set up. The number convergence of iterations used in this analysis was set to 500 and the residual date were set to 1×10^{-6} for greater precision. Simulation control were done in full run with Platform MPI local Parallel mode up to four number of process running. The result obtained from CFD-Post were exported with command editor to analyze the performance of the turbine.

RESULTS AND DISCUSSION

Pseudo and non-dimensional parameters are used to analyse the CFD turbine performance. The pseudo and non-dimensional groups are given below.

Mass Flow Parameter (<i>MFP</i>)	$\frac{\dot{m}\sqrt{T_{01}}}{P_{01}}$
Total-to-static Efficiency	η_{t-s}
Pressure Ratio (<i>PR</i>)	$\frac{P_{01}}{P_3}$
Velocity Ratio	U_2/C_{is}
Speed Parameter (<i>SP</i>)	$\frac{N}{\sqrt{T_{01}}}$

The Total-to-static efficiency, η_{t-s} is the ratio of the actual to the isentropic turbine work output; $\dot{W}_{act}/\dot{W}_{is}$. For the testing data, the \dot{W}_{act} was measured by using eddy current dynamometer and the computational \dot{W}_{act} was measured by the difference of the total enthalpy change between the inlet and outlet turbine flow. The isentropic turbine work, \dot{W}_{is} was calculated by using the isentropic expansion process of the Total Inlet Pressure, P_{02} and the exit static pressure, P_{s3} . The \dot{W}_{is} represents the full energy that can be recovered by the turbine when there are no losses are generated. The *VR* is the ratio of the blade speed, U and the isentropic velocity, C_{is} and the *VR* is inversely proportional with the pressure ratio, *PR*. The turbine performance analysis will be presented in two sections which are; (1) comparison with the testing data 1kW LPT and (2) the turbine performance for various rotational speeds.

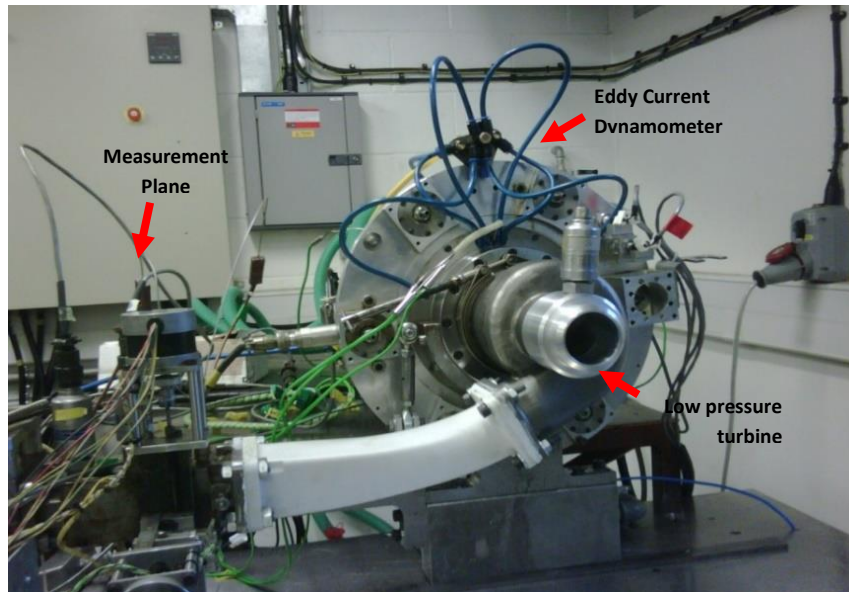


Figure 7. Turbine Assembly on the Eddy current dynamometer in Imperial College turbocharger testing facility [10].

Comparison with the testing of 1 kW data

This section compares the testing data of the 1kW LPT and the CFD data of the 100 kW. The comparison is done for the designed turbine speed which is 50,000 rpm for 1 kW and 5,000 rpm for 100 kW. The testing of the 1 kW LPT turbine was done in Imperial College turbocharger testing facility. The full data for the testing can be find in the reference [10]. Figure 7 shows the experimental set up and the LPT turbine assembly of the Eddy Current dynamometer that is available in the facility. All data such as temperature, inlet pressure and mass flow rate were measured at the measuring plane area.

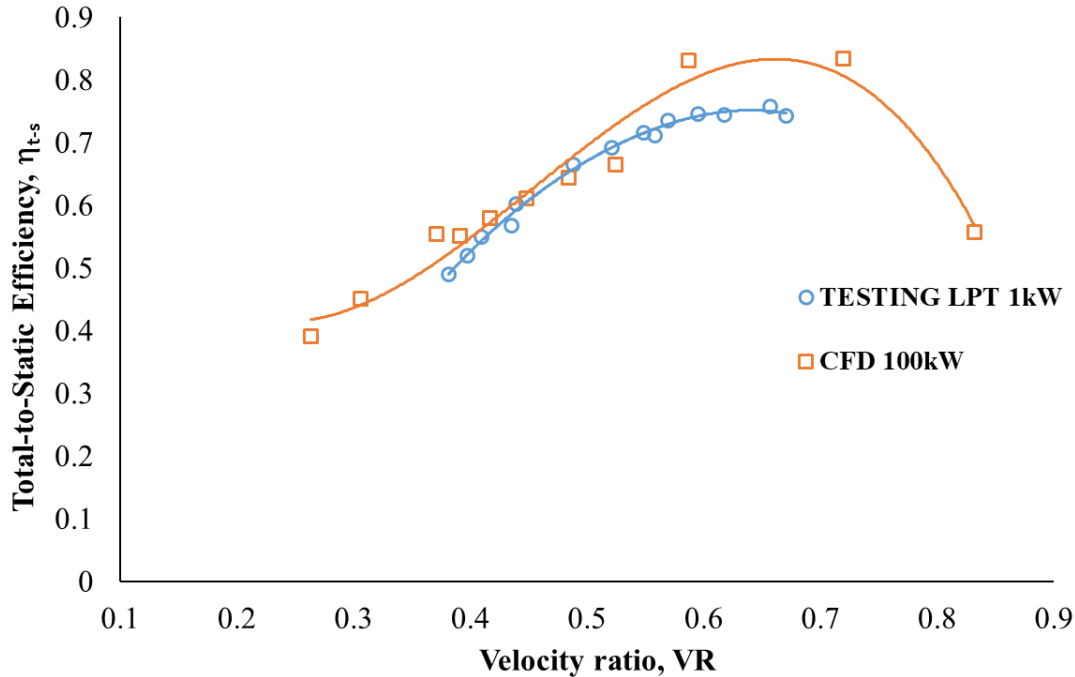


Figure 8. Comparison of turbine performance for the baseline 1.0 kW (experiment) and upscale 100kW (computational).

Figure 8 shows the trend for the total-to-static efficiency, η_{t-s} against the Velocity Ratio, VR. It is shown in the Figure 7 that the location of the peak η_{t-s} is slightly on the higher VR for the CFD LPT 100kW which is approximately at VR = 0.69 and the peak of $\eta_{t-s} = 84\%$. The peak η_{t-s} for the Tested LPT 1kW was deduced at 76% at the VR = 0.66. The Standard Deviation of the total-to-static efficiency, $\sigma_{\eta_{t-s}}$ is 5.4%. The Figure 7 also show that the Total-to-static turbine efficiency for the computational result is higher than the experimental result. This is because the entropy generated in the computational turbine loss is computed by the disorder of the internal flow velocity gradient in the turbine passage only. This is known as passage loss [35]. In the actual turbine operation, the entropy gain in the turbine losses are summed by 4 major turbine losses which are (1) passage loss, caused by shear forces on the turbine surface; (2) friction loss, caused by the velocity gradient in the boundary layer in internal passage; (3) tip clearance loss, caused by the clearance between turbine tips and the shroud volute; and (4) backpressure loss, caused by the flow leakage from the turbine passage to bearing housing [35]. The turbine losses for (2), (3) and (4) could not be computed in the CFD analysis.

The turbine capability to accept the working fluid is known as the turbine swallowing capacity and it is presented by the mass flow parameter, MFP. Figure 9 shows the MFP vs the PR. The x-axis indicates the PR, the primary y-axis is the MFP for the 100 kW scaled LPT using post process from CFD analysis and scaling calculation. The secondary y-axis is the MFP for Testing LPT 1 kW. The scaling calculation for the MFP was obtained by using Equation (5). The Standard Deviation for the MFP between the scaling calculation and the CFD Scaled, σ_{MFP} is 2.05. The Figure 9 shows that the MFP for the 100 kW LPT is 50 times higher than the 1 kW LPT. A similar trend where the turbine will start to choke when the turbine is operated higher than $PR > 1.4$ is found in the Figure 9. The turbine is choked when the working fluid is blocked at the inlet due to high centrifugal force of the turbine rotor. Thus, a higher pressure is developed at the inlet and the working fluid is highly accelerated and expanded in the turbine passage towards the exit of the turbine. A shock wave will develop when the axial velocity Mach number is higher than 1, $Ma_3 > 1$. The turbine will vibrate and might be damaged. Therefore, the turbine testing was not done higher than $PR > 1.3$. In order to avoid from choking, a bypass valve is suggested to be included in the energy recovery system. The bypass will be opened if the $PR > 1.4$ to avoid the LPT from choking and to extend the lifetime of the turbine.

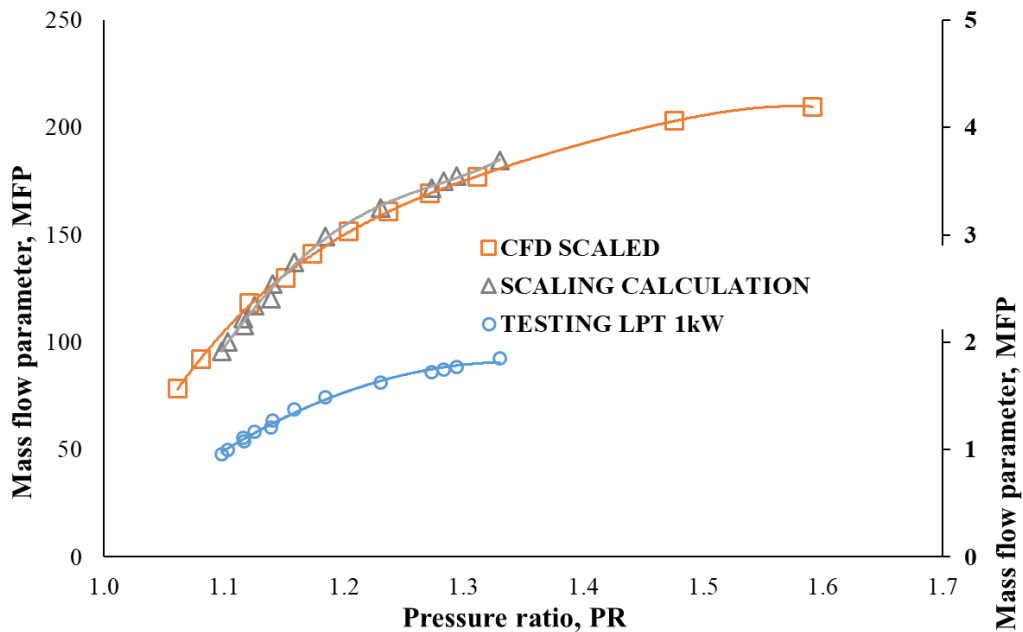


Figure 9. Mass flow capacity characteristics for baseline 1.0 kW (experiment) and upscale 100kW (computational).

The turbine performance for various rotational speeds

The single passage CFD analysis was run for three turbine rotational speeds; 4000 rpm, 5000 rpm and 6000 rpm at steady state condition. This is to represent the off-design operating conditions for the lower speed and higher speed. The pseudo and non-dimensional turbine performance analysis were done in this discussion. The η_{t-s} vs VR performance is given in Figure 10. The maximum η_{t-s} is located in the 5000 rpm speed line. Similar trend for the 4000 rpm and 6000 rpm is found in the Figure 10. The peak η_{t-s} for the 4000 rpm and 6000 rpm is less than the 5000 rpm. It can be observed that the peak η_{t-s} for the lower rotational speed is

shifted to lower VR (or higher PR) and for the higher rotational speed-line, the peak η_{t-s} is shifted to higher VR (or lower PR). This is because the optimum blade velocity triangle is located near to the design point which is approximately 5 kg/s. The discussion of the blade velocity triangle is given in the next section.

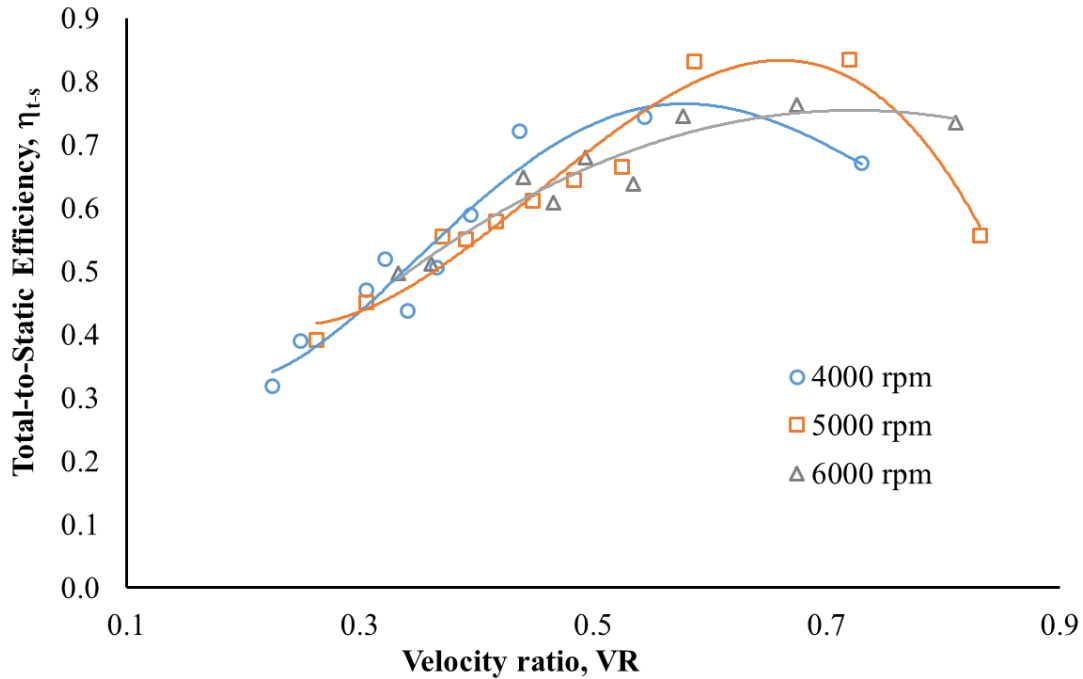


Figure 10. Computational performance for upscale 100 kW turbine at various rotational speeds.

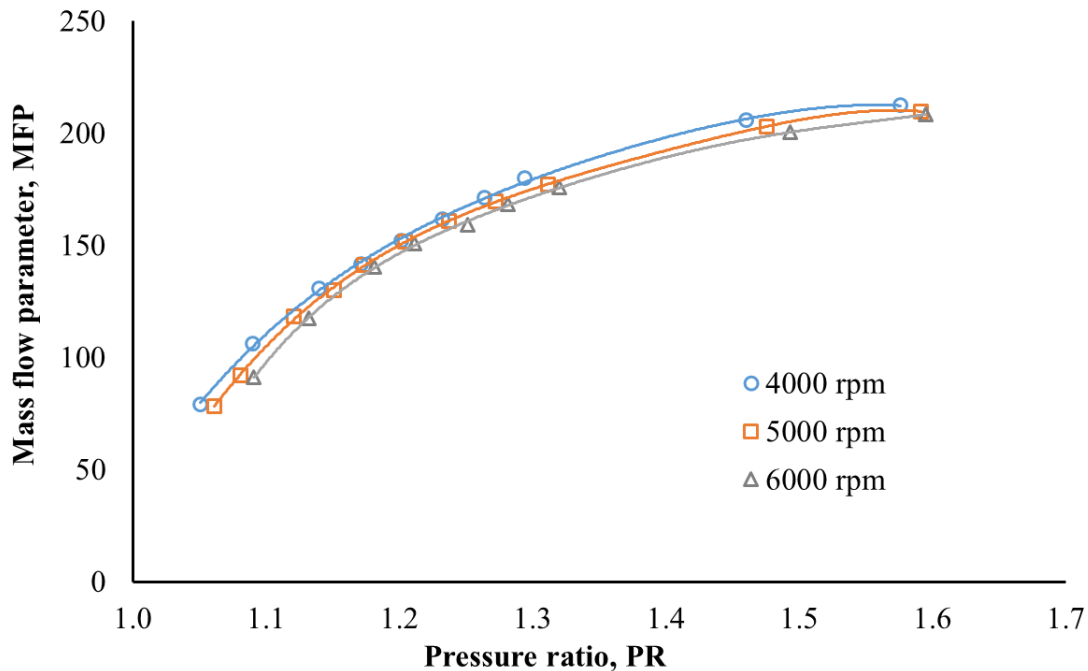


Figure 11. Computational mass flow capacity characteristics for upscale 100kW at various turbine speed.

The swallowing capacity performance for each rotational speed is given in Figure 11. It can be observed that the trend for the swallowing capacity is similar for each operating speed. For a similar PR, the MFP is increased as the turbine speed decreased. This is because the centrifugal force for the low turbine speed is less; subsequently more fluid will swallow into the turbine. Thus, the swallowing capacity is higher for the lower turbine speed. Despite a higher swallowing capacity is obtained for the scaled turbine, the operating PR is still $PR < 1.4$. It can be observed that, for all turbine speeds, the turbine choking will begin at $PR = 1.4$. Therefore, the LPT requires a bypass system to avoid damage and extend its lifetime.

In order to understand the flow characteristics that has contributed to the passage loss in the turbine, Blade Incidence Angle, i effect in the turbomachinery velocity triangle at the leading edge of the turbine blade can be analysed. The Blade Incidence Angle, i is an angle between the Relative Flow Angle, β_2 and the Blade Angle, β_b (refer to the Figure 3(b)). The maximum turbine total-to-static, η_{t-s} is located at $VR \approx 0.69$. It can be seen from Figure 12 that, the optimum Blade Incidence Angle, i is between -30° and -40° for all rotational turbine speeds. This result is similar to the fundamental discussion by Japikse & Baines where the optimum turbine efficiency is in the range of in the range of -30° to -40° [35]. As the PR is increased in the off-design operating condition at constant rotational turbine, the mass flow rate and the isentropic velocity, C_{is} is increased; consequently the VR is decreased. This will increase the meridional velocity, C_{m2} and the Absolute Angle, α_2 and decrease the Relative Angle at the leading edge, β_2 . As a result, the Incidence Angle, i is increased as the VR is decreased. This behaviour can be seen clearly in the Figure 12.

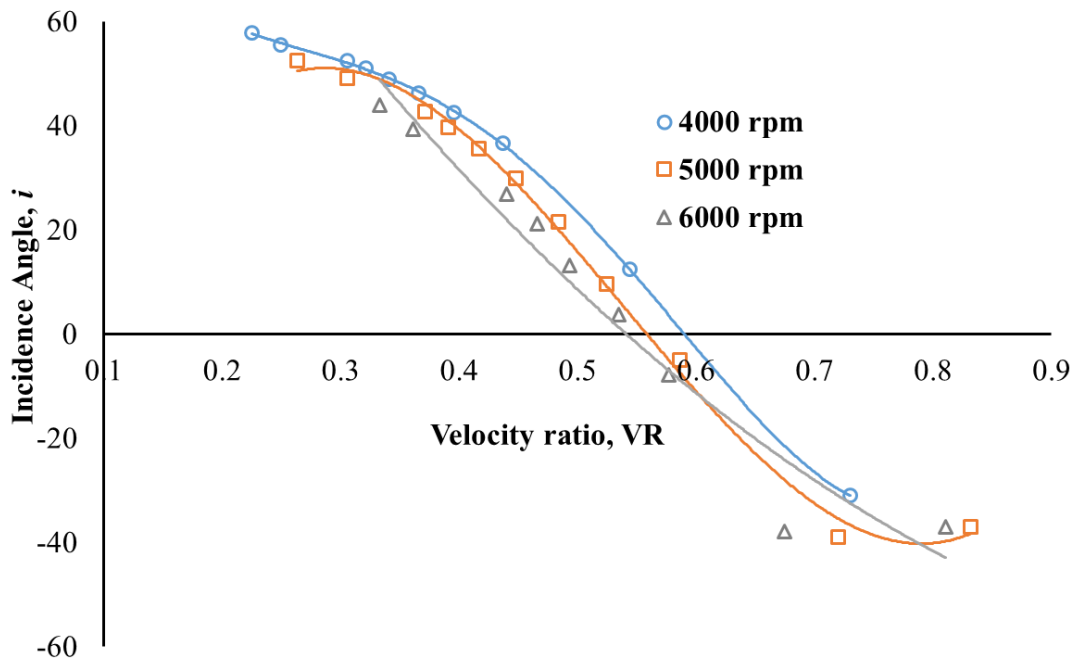


Figure 12. Blade incidence angle, i against the velocity ratio, VR .

CONCLUSION

This paper has proven that the turbine scaling method can be used to increase the turbine capacity. The first objective of this paper which is to obtain a physical parameter for the 100kW LPT was achieved by the numerical scaling process. By using the scale factor, f of 10. The turbine speed is reduced from 50,000 rpm to 5,000 rpm and the mass flow rate is increased from 0.05 kg/s to 5.0 kg/s due to the diameter scaling effect for the 100 kW turbine. The CFD analysis has shown that the peak efficiency of the turbine performance is obtained approximately 81% at the VR of 0.68. The velocity triangle for the turbine rotor is maintained. It is found that the optimum Incidence Angle, i is approximately -40° when the total-to-static efficiency achieved its maximum value. The turbine turbine swallowing capacity is limited below than 1.4 to avoid turbine choking. In conclusion, the application of turbine scaling method can preserve the turbine flow characteristics because the turbine losses and the swallow capacity for the baseline and upscale turbine are similar.

ACKNOWLEDGEMENT

The authors would like to thank Universiti Teknologi MARA (UiTM) and the Ministry of Education (MOE) for its financial funding of this research under the Fundamental Research Grant Scheme (FRGS) File #: 600-RMI/FRGS 5/3 (71/2013).

REFERENCES

- [1] International Energy Agency. World energy outlook 2018. Retrieved from <https://webstore.iea.org/download/summary/190?fileName=English-WEO-2018-ES.pdf>; 13 November, 2018.
- [2] Chiara F, Canova M. A review of energy consumption, management, and recovery in automotive systems, with considerations of future trends. Proceedings of the Institution of Mechanical Engineers, Part D: Journal of Automobile Engineering 2013;227:914-936.
- [3] Sasongko MN, Wijayanti W. Effect of ethanol addition on the performance and exhaust emissions of a spark ignition engine. Journal of Mechanical Engineering and Sciences 2017;11:2734-2742.
- [4] Boretti A, Al-Zubaidy S. E-KERS Energy management crucial to improved fuel economy. SAE Technical Papers: 016-01-1947; 2016 .
- [5] Fennell D, Herreros J, Tsolakis A. Improving gasoline direct injection (GDI) engine efficiency and emissions with hydrogen from exhaust gas fuel reforming. International Journal of Hydrogen Energy 2014;39:5153-5162.
- [6] Matulić N, Radica G, Nižetić S. Thermodynamic analysis of active modular internal combustion engine concept: Targeting efficiency increase and carbon dioxide emissions reduction of gasoline engines. International Journal of Energy Research 2018;42:3017-3029.
- [7] Treffinger P, Häfele C, Weiler T, Eder A, Richter R, Mazar B. Energy recovery by conversion of waste heat into useful energy. VDI Berichte, 2008: 385-405.

- [8] Armstead JR, Miers SA. Review of waste heat recovery mechanisms for internal combustion engines. American Society of Mechanical Engineers, Internal Combustion Engine Division (Publication) 2010; 965-974.
- [9] Pavlas M, Touš M. Efficient waste-to-energy system as a contribution to clean technologies. Clean Technologies and Environmental Policy 2009;11:19-29.
- [10] Bin Mamat AMI, Martinez-Botas RF, Rajoo S, Hao L, Romagnoli A. Design methodology of a low pressure turbine for waste heat recovery via electric turbocompounding. Applied Thermal Engineering 2016;107:1166-1182.
- [11] Bin Mamat AMI, Martinez-Botas RF, Rajoo S, Romagnoli A, Petrovic S. Waste heat recovery using a novel high performance low pressure turbine for electric turbocompounding in downsized gasoline engines: Experimental and computational analysis. Energy 2015;90:218-234.
- [12] Nawi MRM, Mamat AMI, Ismail H. Numerical heat transfer analysis of waste heat exchanger for exhaust gas energy recovery. Journal of Mechanical Engineering and Sciences 2015;8:1498-1506.
- [13] Ababneh M, Al-Jarrah AA, Sha'ban H, BaniHani S, Al-Jarrah AM, AlMomani T, et al. Recovering waste heat from automobile engine using thermoelectric power generators. International Review of Mechanical Engineering 2017;11:845-854.
- [14] Aghaali H, Ångström HE. A review of turbocompounding as a waste heat recovery system for internal combustion engines. Renewable and Sustainable Energy Reviews 2015;49:813-824.
- [15] Alshammari F, Karvountzis-Kontakiotis A, Pesyridis A, Usman M. Expander technologies for automotive engine organic rankine cycle applications. Energies 2018;11:1-36.
- [16] Fu G, Zuo L, Longtin JP. Review of waste energy resource in vehicle engine exhaust. In: ASME 2012 Heat Transfer Summer Conf Collocated with the ASME 2012 Fluids Engineering Div Summer Meeting and the ASME 2012 10th Int Conf on Nanochannels, Microchannels and Minichannels, Puerto Rico, USA, 8–12 July, 2012.
- [17] Andwari AM, Pesiridis A, Esfahanian V, Salavati-Zadeh A, Karvountzis-Kontakiotis A, Muralidharan V. A comparative study of the effect of turbocompounding and ORC Waste Heat Recovery systems on the performance of a turbocharged heavy-duty diesel engine. Energies. 2017;10:1-17.
- [18] Sakellariadis NF, Antonopoulos AK, Pariotis EG, Hountalas DT. Model-based theoretical optimization study of a turbo-compound system installed on a large scale marine diesel engine. Turbochargers and Turbocharging: Advancements, Applications and Research, 2017: 55-90.
- [19] Walsh P, Gas turbine performance. 2nd ed. U.S.A.: Blackwell Science; 2004.
- [20] Hountalas DT, Knecht W, Zannis TC. Exhaust heat recuperation from dl diesel engines using mechanical and electrical turbocompounding. In: The 23rd International Conference on Efficiency, Cost, Optimization, Simulation, and Environmental Impact of Energy Systems, Lausanne, Switzerland, pp. 53-61; 2010.
- [21] Bin Mamat AMI, Romagnoli A, Martinez-Botas RF. Characterization of a low pressure turbine for turbocompounding applications in a mild-hybrid gasoline engine. In : 10th International Conference on Turbochargers and Turbocharging, London, United Kingdom, pp. 281-93; 2010.

- [22] Briggs I, McCullough G, Spence S, Douglas R. Whole-vehicle modelling of exhaust energy recovery on a diesel-electric hybrid bus. *Energy*. 2014;65:172-81.
- [23] Mingshan W, Jinli F, Chaochen M, Noman DS. Waste heat recovery from heavy-duty diesel engine exhaust gases by medium temperature ORC system. *Science China Technological Sciences*. 2011;54:2746-2753.
- [24] Briggs I, McCullough G, Spence S, Douglas R, O'Shaughnessy R, Hanna A. Waste heat recovery on a diesel-electric hybrid bus using a turbogenerator. *SAE Technical Papers: 2012-01-1945*; 2012.
- [25] Teo AE, Yahya WJ, Romagnoli A, Rajoo S, Noor AM. Effectiveness of series and parallel turbo compounding on turbocharged diesel engine. *Journal of Mechanical Engineering and Sciences* 2015;8:1448-1459.
- [26] He G, Xie H, Gu Z. Investigation into Comprehensive Fuel Saving Potential of Diesel with Electric Turbo-compounding Waste Heat Recovery Power Generation and Electric Thermal Management Power Consumption Systems. *Hsi-An Chiao Tung Ta Hsueh/Journal of Xi'an Jiaotong University* 2017;51:112-120.
- [27] Deshmukh DS, Modak JP, Nayak KM. Experimental analysis of backpressure phenomenon consideration for C.I. engine performance improvement. *SAE Technical Papers: 2010-01-1575*, 2010.
- [28] Terdich N, Martinez-Botas RF, Romagnoli A, Pesiridis A. Mild hybridization via electrification of the air system: electrically assisted and variable geometry turbocharging impact on an off-road diesel engine. *Journal of Engineering for Gas Turbines and Power*. 2014;136(3):1-12.
- [29] Romagnoli A, Manivannan A, Rajoo S, Chiong MS, Feneley A, Pesiridis A. A review of heat transfer in turbochargers. *Renewable and Sustainable Energy Reviews* 2017;79:1442-1460.
- [30] Zhao R, Li W, Zhuge W, Zhang Y, Yin Y. Numerical study on steam injection in a turbocompound diesel engine for waste heat recovery. *Applied Energy* 2017;185:506-518.
- [31] Kant M, Romagnoli A, Mamat AM, Martinez-Botas RF. Heavy-duty engine electric turbocompounding. *Proceedings of the Institution of Mechanical Engineers, Part D: Journal of Automobile Engineering* 2015;229:457-472.
- [32] Ahmad B, Fattah A, Bin Mamat AMI. Single passage CFD analysis for non radial fibre element of low pressure turbine. *Jurnal Teknologi* 2015;76:67-72.
- [33] Liang X, Wang X, Shu G, Wei H, Tian H, Wang X. A review and selection of engine waste heat recovery technologies using analytic hierarchy process and grey relational analysis. *International Journal of Energy Research* 2015;39:453-471.
- [34] Roque Díaz P, Benito YR, Parise JAR. Thermo-economic assessment of a multi-engine, multi-heat-pump CCHP (combined cooling, heating and power generation) system - A case study. *Energy* 2010;35:3540-3550.
- [35] Japikse D, Baines NC. *Introduction to turbomachinery*. 1st Ed. Vermont, USA: Oxford University Press; 1994.